

## Article

# Effect of Colorants and Process Parameters on the Properties of Dope-Dyed Poly(lactic Acid) Multifilament Yarns

Naveen Kumar Balakrishnan <sup>1</sup>, Stefan Siebert <sup>1</sup>, Christoph Richter <sup>2</sup>, Robert Groten <sup>2</sup> and Gunnar Seide <sup>1,\*</sup>

<sup>1</sup> Aachen-Maastricht Institute for Biobased Materials (AMIBM), Maastricht University, Brightlands Chemelot Campus, Urmonderbaan 22, 6167 RD Geleen, The Netherlands

<sup>2</sup> Department of Textile and Clothing Technology, Niederrhein University of Applied Sciences, Campus Moenchengladbach, Webschulstrasse 31, 41065 Moenchengladbach, Germany

\* Correspondence: [gunnar.seide@maastrichtuniversity.nl](mailto:gunnar.seide@maastrichtuniversity.nl)

**Abstract:** The color of textile fibers is typically imparted by submersion in a high-temperature dye bath. However, the treatment of the effluent is challenging and the textile industry is therefore a major source of water pollution. Current fashion trends favor biobased polymers such as poly(lactic acid) (PLA) but exhaust dyeing at high temperatures causes hydrolytic degradation, reducing the crystallinity and tenacity of the yarn. To preserve the mechanical properties of PLA-based textiles, an alternative to exhaust dyeing called dope dyeing can be used, wherein colorants are incorporated into the polymer matrix during melt spinning. We evaluated this process by dope dyeing PLA with several colorants, then testing the thermal, physical, and mechanical properties of the yarn and the physical properties of circular-knitted fabrics. Although the colorants affected the crystallization behavior at lower cooling rates, during the melt-spinning process, the drawing speed had a greater effect on the crystallinity and mechanical properties of the dyed yarn. Scanning electron microscopy revealed that the colorants were well dispersed in the PLA matrix. We found that the colorants did not affect the physical properties of the knitted fabric. Our results can be used to develop more environmentally beneficial dope-dyed PLA yarn with improved mechanical properties.

**Keywords:** fiber spinning; dope dyeing; nucleating agent; crystallinity; sustainability; biobased polymer; biopolymer processing; biobased textiles



**Citation:** Balakrishnan, N.K.; Siebert, S.; Richter, C.; Groten, R.; Seide, G. Effect of Colorants and Process Parameters on the Properties of Dope-Dyed Poly(lactic Acid) Multifilament Yarns. *Polymers* **2022**, *14*, 5021. <https://doi.org/10.3390/polym14225021>

Academic Editor: Md. Arifur Rahim

Received: 9 October 2022

Accepted: 16 November 2022

Published: 19 November 2022

**Publisher's Note:** MDPI stays neutral with regard to jurisdictional claims in published maps and institutional affiliations.



**Copyright:** © 2022 by the authors. Licensee MDPI, Basel, Switzerland. This article is an open access article distributed under the terms and conditions of the Creative Commons Attribution (CC BY) license (<https://creativecommons.org/licenses/by/4.0/>).

## 1. Introduction

Synthetic fiber production has doubled in the last two decades, reaching 80.9 million tonnes in 2020, and the most common material is poly(ethylene terephthalate) (PET), accounting for 48 million tonnes [1]. Because PET is an oil-based polymer, its production from nonrenewable raw material, and its ultimate disposal contribute to climate change. The textile industry is therefore shifting towards more sustainable and biobased and/or biodegradable polymers, which reached a production volume of 2.11 million tonnes in 2020, with poly(lactic acid) (PLA) accounting for 18.7% of this total [2]. PLA can be produced from renewable resources such as corn, sugar beet, and wheat, and it currently accounts for less than 0.03% of global corn production, thus representing negligible competition with food crops. Although often described as biodegradable, PLA is only compostable under industrial conditions [3]. The production of 1 tonne of PLA consumes 42 GJ of energy and releases 1.3 tonnes of CO<sub>2</sub>, ~40% less than PET [4]. Furthermore, PLA fibers are characterized by inherently better moisture management, a higher limiting oxygen index (LOI), and enhanced wicking properties compared to PET fibers, making them suitable for use in sustainable clothing [5].

Despite the advantages of PLA, its commercial production is limited by its thermolability and low heat resistance due to its glass transition temperature ( $T_g$ ) of ~55 °C [6]. The heat resistance of PLA can be improved by increasing its crystallinity, but the inherent low

crystallization rate of the polymer leads to products with low crystallinity, which hinders conventional exhaust dyeing [7,8]. PET is exhaust dyed at 130 °C without loss of integrity, but PLA is hydrolyzed under these conditions, weakening the fibers [9]. However, dyeing at lower temperatures results in poor dye take-up compared to PET [3,10,11]. The exhaust dyeing of PLA with indigoid compounds is possible at 110 °C [11,12]. Furthermore, PLA fibers modified with polyhedral oligomeric silsesquioxane nanoparticles also showed better dyeability than pure PLA [13]. The dyeing of recycled PLA fibers using selected disperse dyes achieved satisfactory exhaustion rates at 80 °C, but the light fastness of the fibers was poor [10]. Natural dye from flowers has also been used to produce yellow PLA films [14]. The tensile strength of PLA declines with increasing dyeing time, probably reflecting the impact on fiber crystallinity [6,15].

Despite its widespread use, conventional exhaust dyeing is unsustainable because toxic chemicals are needed to fix colorants to the polymer and on top of it, 10–25% of the dye is lost during the process, 2–20% of which is directly discharged into rivers and streams along with the toxic fixatives [16]. The textile industry is therefore the second greatest global polluter of water resources [17]. Exhaust dyeing at high temperatures also consumes energy, and the high temperatures not only cause the degradation of labile fibers such as PLA but also affect crystallinity and lead to shrinkage, disrupting the fiber orientation [6]. In comparison, mass coloration or dope dyeing involves the incorporation of colorants into the polymer melt during fiber production [18]. The dope dyeing of PLA with carbon black was shown to improve the mechanical properties of the fibers [19]. A comparison of dope dyeing and exhaust dyeing of polyamide 6 revealed that dope dyeing reduces water use by ~40%, chemical use by 97%, and waste by ~50% and also reduces the overall number of processing steps [20].

Although dope dyeing has many advantages, only 5% of polyester fibers are dope dyed, and the proportion is even lower for PLA [18]. Like PLA, polypropylene (PP) is also characterized by slow crystallization, but this has been controlled and optimized by using colorants as nucleating agents [21]. We recently reported a similar nucleating effect when using selected pigments in PLA [22]. However, the effect of colorants on the mechanical, rheological, and thermal properties of PLA during dope dyeing has not been studied in detail. Herein, we describe the dope dyeing of PLA with fossil-based and biobased colorants. We compared the biobased pigment pink PR122 and the potential biobased colorant alizarin to the fossil-based pigments green 7, blue 15:1, and yellow 155. We incorporated different weight percentages of the colorants into PLA melts and determined their effect on the rheological and thermal properties of yarn, including their propensity for degradation. We also used different draw ratios to investigate the influence of additives and process parameters on the mechanical properties and crystallinity of the PLA yarns. Finally, we prepared circular-knitted fabrics from the melt-spun yarns and investigated their air permeability, water vapor permeability, and Martindale abrasion resistance. We compared the performance of the different colorants to assess the potential of biobased colorants for the development of environmentally beneficial dope-dyed PLA yarns with improved properties.

## 2. Materials and Methods

### 2.1. Materials

PLA grade L130 (TotalEnergies-Corbion, Gorinchem, Netherlands) was used for all experiments and has the following manufacturer-specified properties: L-content  $\geq 99\%$ ,  $T_g \sim 60$  °C, and melt flow index = 24 g/10 min at 210 °C/2.16 kg. We purchased alizarin (Sigma-Aldrich, St Louis, MO, USA), whereas the pigments blue 15:1, green 7, pink PR122, and pigment yellow 155 were kindly donated by Clariant (Muttenz, Switzerland). The chemical structure of the colorants are presented below in Table 1.

**Table 1.** Chemical structure of the colorants [23–27].

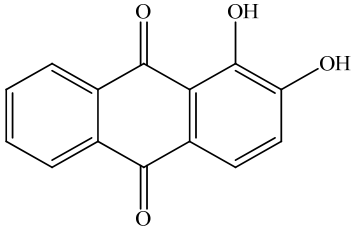
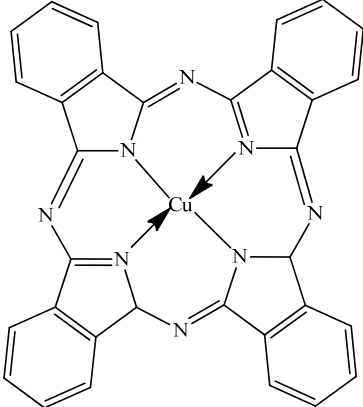
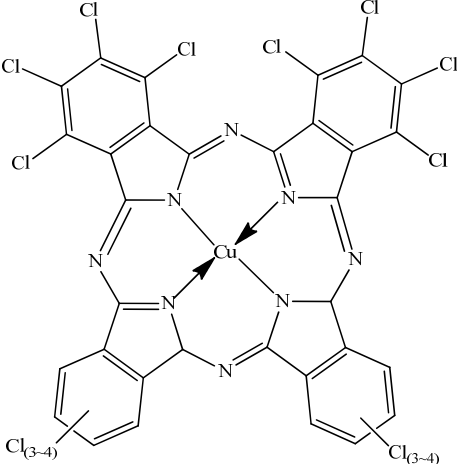
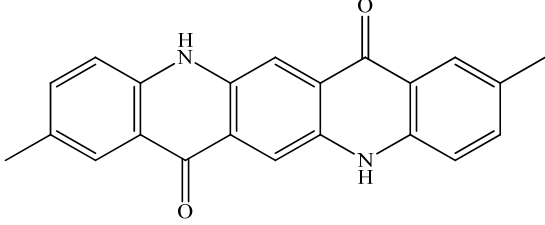
Additive	Chemical Structure
Alizarin	 <p>The structure shows a central carbon atom bonded to three phenyl rings. Two of the phenyl rings are substituted with hydroxyl groups (-OH) at the 1 and 2 positions. The central carbon is also bonded to two oxygen atoms, one above and one below, forming a quinone-like structure.</p>
Pigment blue 15:1	 <p>The structure shows a central copper atom (Cu) coordinated to four nitrogen atoms in a square planar arrangement. Each nitrogen atom is part of a benzene ring, forming a phthalocyanine-like macrocycle.</p>
Pigment green 7	 <p>The structure shows a central copper atom (Cu) coordinated to four nitrogen atoms in a square planar arrangement. Each nitrogen atom is part of a benzene ring. The benzene rings are substituted with chlorine atoms (Cl) at the 3 and 4 positions, indicated by the label Cl(3-4).</p>
Pink PR122	 <p>The structure shows a central quinacridone core consisting of three fused benzene rings and one fused naphthalene ring. The naphthalene ring is substituted with a methyl group (-CH3) at the 1 position. The quinacridone core is also substituted with a methyl group (-CH3) at the 8 position.</p>

Table 1. Cont.

Additive	Chemical Structure
Pigment yellow 155	

### 2.2. Compounding

We dried PLA and the colorants under a vacuum at 80 °C overnight to reduce the moisture content. The materials were compounded using a KETSE 20/40 twin-screw extruder (Brabender, Duisburg, Germany) with a screw diameter (D) of 20 mm and a length of 40D. Master batches containing 5% (*w/w*) of each colorant were prepared (named A5, B5, G5, P5, and Y5). The extrudates were cooled in a water bath before granulation.

### 2.3. Melt Spinning

Fibers were prepared using an FET-100 series pilot-scale melt-spinning machine (Fibre Extrusion Technology, Leeds, UK) featuring a spinneret with 48 holes (diameter 0.25 mm) and an L/D ratio of 2 (Figure 1). The materials were dried again at 80 °C overnight under vacuum before spinning at a temperature of 200 °C. We maintained a constant extruder pressure of 60 bars and a constant throughput of 45 g/min at a winding speed of 1200 m/min, but we applied three different draw ratios.

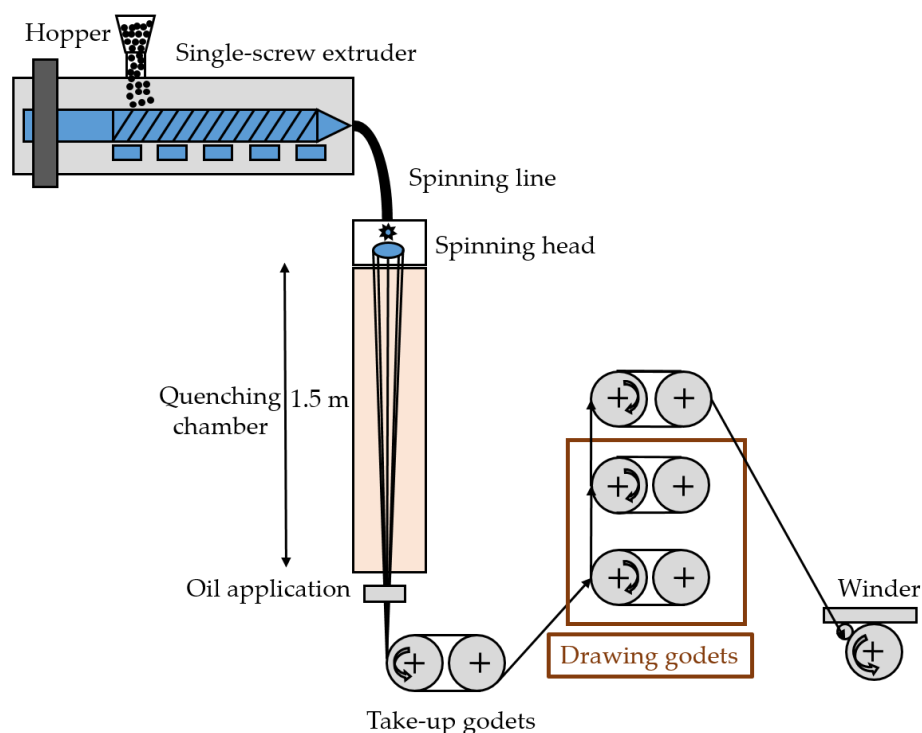


Figure 1. Schematic illustration of the pilot-scale melt-spinning device.

The master-batch granules were diluted with pure PLA to achieve weight-percentages of 0.1%, 0.2%, and 0.3% for melt spinning. The first yarn was drawn fully from the melt, and no solid-state drawing (SSD) was applied. The second yarn was semi-drawn from the melt (medium SSD). The third yarn was only slightly drawn from the melt and was primarily drawn by SSD. We compared yarns produced with the highest weight percentage of colorants (0.3%) because, if no significant effects were observed at this concentration, we could rule out effects at lower concentrations without testing. The yarns were named using the convention C0x.y, wherein C is the first letter of the colorant name, x is the weight percentage, and y is the SSD ratio. For example, PLA.1 refers to the pure PLA yarn drawn with an SSD ratio of 1, and A03.2 refers to the yarn dyed with 0.3% (*w/w*) alizarin and drawn with an SSD ratio of 2. The complete set of yarns is presented in Table 2.

**Table 2.** Complete set of yarns produced under different experimental parameters.

Abbreviation	Material: Colorants Shown as % ( <i>w/w</i> )	Take-Up (m/min)	Melt-Drawing Ratio	Winding Speed (m/min)	SSD Ratio
PLA.1	PLA	1100	72	1200	1
PLA.2	PLA	600	39	1200	2
PLA.3	PLA	400	26	1200	3
A03.1	PLA + 0.3% alizarin	1100	72	1200	1
A03.2	PLA + 0.3% alizarin	600	39	1200	2
A03.3	PLA + 0.3% alizarin	400	26	1200	3
B03.1	PLA + 0.3% blue 15:1	1100	72	1200	1
B03.2	PLA + 0.3% blue 15:1	600	39	1200	2
B03.3	PLA + 0.3% blue 15:1	400	26	1200	3
G01.1	PLA + 0.3% green 7	1100	72	1200	1
G02.2	PLA + 0.3% green 7	600	39	1200	2
G03.3	PLA + 0.3% green 7	400	26	1200	3
P03.1	PLA + 0.3% pink PR122	1100	72	1200	1
P03.2	PLA + 0.3% pink PR122	600	39	1200	2
P03.3	PLA + 0.3% pink PR122	400	26	1200	3
Y03.1	PLA + 0.3% yellow 155	1100	72	1200	1
Y03.2	PLA + 0.3% yellow 155	600	39	1200	2
Y03.3	PLA + 0.3% yellow 155	400	26	1200	3

#### 2.4. Knitting

The melt-spun yarn was knitted using a TK-83 circular knitting machine (Harry Lucas, Neumünster, Germany). A knitted fabric with a single jersey structure was produced on gauge E24/gg using 264 needles with a cylinder diameter of 3½ inches. A knitted fabric was prepared from PLA and dyed PLA yarns produced at an SSD ratio of 1 and a colorant content of 0.3% (*w/w*). All fabrics were prepared using the same knitting parameters (stitch, take-off, and knitting speed).

#### 2.5. Characterization of Colorants

Differential scanning calorimetry (DSC) was used to reveal any thermal transitions during processing. We applied one heating and one cooling cycle from 25 °C and 250 °C at a heating rate of 10 °C/min using a SC 214 device (Netzsch, Selb, Germany). The morphology of the colorants was determined by scanning electron microscopy (SEM) using a JSM-IT200 device (Jeol, Freising, Germany). The images were acquired in secondary electron mode with an acceleration tension of 15 kV and are presented at 1000× magnification.

#### 2.6. Characterization of Master Batches

The masterbatches of PLA with 5% (*w/w*) of colorants were analyzed by DSC from 25 °C to 200 °C to investigate the effect of colorants on thermal transition temperatures. We applied two heating cycles and one cooling cycle. We used the second heating cycle to determine the effect of colorants on any change in thermal transition, and we used the first

cooling cycle to investigate any change in crystallization temperature ( $T_c$ ). The  $T_g$ , melting point ( $T_m$ ) and cold crystallization temperature ( $T_{cc}$ ) were also compared.

Rheological analysis was carried out using a Discovery Hybrid Rheometer (DHR1) from TA Instruments (New Castle, DE, USA). Angular frequencies were applied over the range 1 to 624 rad/s using a 25 mm plate plate setup to investigate the effect of colorants on the viscosity of PLA, and complex viscosity values were compared at the same angular frequency (10 rad/s).

Fourier-transform infrared (FTIR) spectroscopy was used to investigate interactions between PLA and the colorants. FTIR spectra were recorded on a PerkinElmer 400 FT(N)IR device (Waltham, MA, USA) in transmission mode by completing 64 scans between 4000 and 500/cm with a resolution of 2/cm.

The cross-section of the master batches was analyzed by SEM as described above to determine the distribution of colorants. The samples were frozen in liquid nitrogen, fractured, and sputtered with gold prior to the measurements.

The average molecular weight ( $M_n$ ), weight average molecular weight ( $M_w$ ), and polydispersity index (PDI) of PLA and its master batches were determined by gel permeation chromatography (GPC) using a 1260 Infinity device (Agilent Technologies, Santa Clara, CA, USA). The mobile phase was hexafluoro-2-isopropanol (HFIP) containing 0.19% sodium trifluoroacetate. We prepared filtered solutions containing 5 mg samples and injected them into a 7  $\mu\text{m}$  modified silica column. We used a standard polymethyl methacrylate polymer ( $1.0 \times 10^5$  g/mol) for calibration.

### 2.7. Characterization of Yarn

DSC over the range 35 to 200 °C was used to determine the effect of colorants, their weight percentage, and the drawing parameters on the thermal transitions of PLA yarn. We measured the  $T_g$ ,  $T_m$ , and  $T_{cc}$  and the degree of crystallinity ( $X_c$ ) of pure PLA and dyed PLA yarns. The melting enthalpy of 100% crystalline PLA is 93.7 J/g [28–30].

The yarn linear density (weight per length) was measured according to DIN EN ISO 1973, and mechanical properties (tenacity and elongation) were measured using a ZwickLine Z2.5 instrument (Zwick Roell, Ulm, Germany) according to DIN EN ISO 2062. A starting length ( $L_0$ ) of 200 mm was used, and the test was carried out at 200 mm/min. All tests were carried out in triplicate.

Commission Internationale de l'Éclairage (CIE)  $L^*a^*b^*$  color coordinates were measured using a PCE CSM 7 colorimeter (PCE Instruments, Palm Beach, FL, USA) according to EN ISO 11664-4. An aperture size of 4 mm was used.  $L^*$  is the lightness index and can vary from 0 (black) to 100 (white); a higher negative  $a^*$  value indicates a stronger green color; a higher positive  $a^*$  value indicates a stronger red color. Similarly, a higher negative  $b^*$  value indicates a stronger blue color, and a higher positive  $b^*$  value indicates a stronger yellow color.

The ultraviolet (UV) light stability of the colorants in dyed yarns was measured using a blue wool scale (BWS) test according to ISO 105-B02. We exposed the samples to UVA light ( $0.68 \text{ W/m}^2$ ) at 340 nm and 50 °C. We prepared sample swatches from the yarn dyed with 0.3% ( $w/w$ ) of each colorant, and the CIE  $L^*a^*b^*$  coordinates were measured on the left, middle, and right. The middle part of the sample was always covered to prevent UV exposure. Samples showing a visual change at level 4 of the grayscale were given a preliminary score. The left part was then covered. The test was continued, and a final score was given when the right part matched level 3 of the grayscale. After 130 h, we evaluated the effect of the UV on the samples. At this point, we graded light-fastness against the BWS and assigned a score between 1 (very poor) and 8 (excellent).

### 2.8. Characterization of Knitted Fabric

The effect of the colorants on the air permeability and water vapor permeability of knitted fabrics was investigated using an FX 3300 tester (Textest Instruments, Schwerzenbach, Switzerland) and Permetest (Sensora, Liberec, Czech Republic). Air permeability

was measured on all knitted fabrics with an air pressure of 200 Pa and a test area of 20 cm<sup>2</sup> according to DIN EN ISO 9237. Water vapor permeability was measured according to DIN EN ISO 11092. Abrasion resistance was measured using an AquAbrasion 1819 Martindale abrasion test device (James Heal, Sterling, VA, USA). The test was carried out according to DIN EN ISO 12947-2 with 15,000 cycles. After 1000, 2000, 3000, 4000, 5000, 7500, and 10,000 cycles, the test was stopped, and images were captured to record the abrasion of the knitted fabric. The CIE L\*a\*b\* color coordinates of the fabric were also measured, according to the procedure mentioned above, before, and after the Martindale test to determine the abrasion resistance of the colorants. Five samples of each knitted fabric were tested at a nominal pressure of 12 kPa.

### 3. Results and Discussion

#### 3.1. Analysis of the Colorants

##### 3.1.1. Thermal Characteristics

Most colorants showed little to no thermal transition under our experimental conditions, as anticipated because their  $T_m$  lay beyond the tested temperature range (Figure 2). Even so, we observed a broad endothermic peak between 50 and 100 °C for the blue 15:1 and green 7 colorants and alizarin. Given that the two inorganic colorants were not dried before DSC and are based on copper complexes, this could indicate the evaporation of residual water. Similarly, the peak observed in the alizarin thermogram was assumed to represent water evaporation because the colorant is not expected to undergo other thermal transitions within this temperature range. Similar observations have been reported for TiO<sub>2</sub> [31]. No significant peak was observed for any of the colorants during the cooling cycle. We used a temperature of 200 °C for the melt spinning of PLA, and no thermal transition was observed for any of the colorants below 200 °C, so no change in the physical state of the colorants was anticipated during melt spinning.

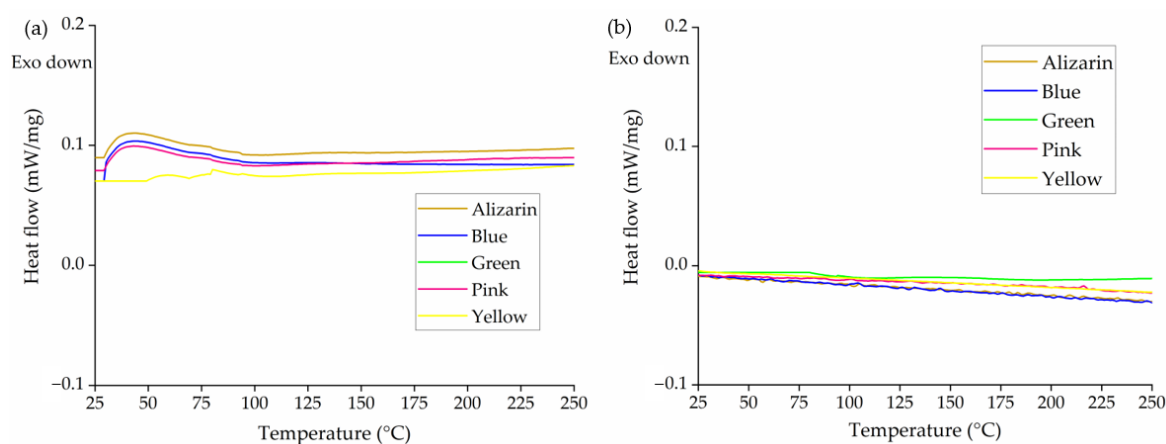


**Figure 2.** DSC thermograms of five colorants during (a) the heating cycle and (b) the cooling cycle.

##### 3.1.2. Morphological Characteristics

The colorants are supplied as tiny crystals in the shape of bricks, rods, or plates, but this structure can break down during processing due to the high temperature and/or shear forces, and the crystals can also dissolve in the surrounding medium [32]. SEM images revealed that alizarin has a needle-like structure, whereas the blue 15:1, green 7, and yellow 155 pigments have a plate-like structure, and pigment pink PR122 has a spherical morphology (Figure 3). All five colorants formed agglomerates, ranging in size from ~2 μm (blue 15:1, green 7 and yellow 155) to 2–5 μm (pink PR122) and 10–20 μm (alizarin).

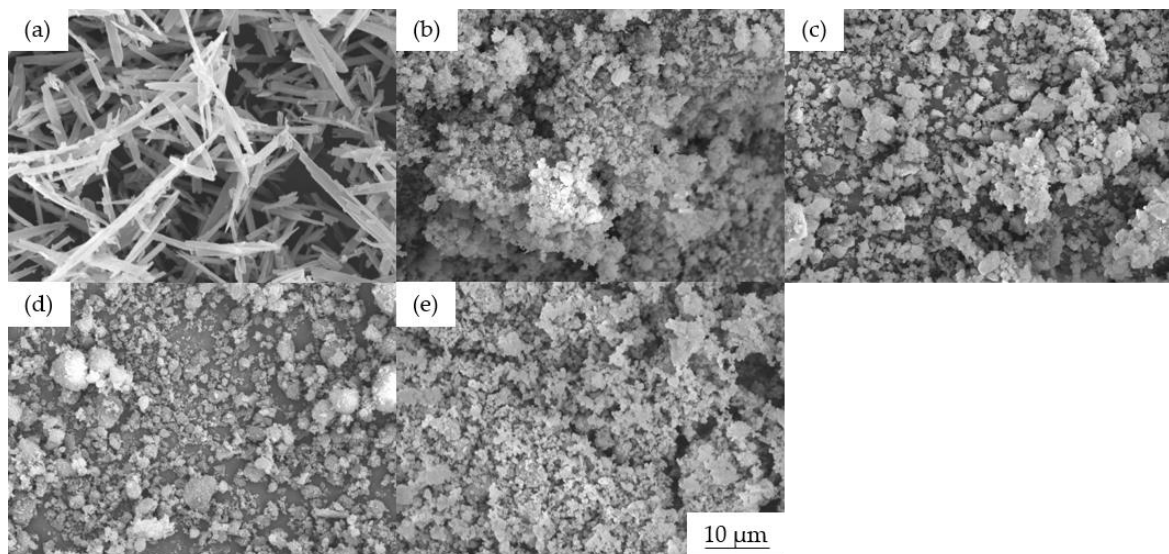


**Figure 3.** SEM images of the colorants (a) alizarin, (b) pigment blue 15:1, (c) pigment green 7, (d) pigment pink PR122, and (e) pigment yellow 155.

### 3.2. Analysis of PLA Master Batches

#### 3.2.1. Thermal Characteristics

The DSC thermograms of PLA and its master batches containing 5% (*w/w*) of each colorant (A5, B5, G5, P5, and Y5) are presented in Figure 4. PLA and all five master batches showed a major melting peak at  $\sim 175$  °C. However, master batches G5 and P5 also showed a second, minor melting peak at  $\sim 165$  °C, which may indicate a defective crystal structure. The defective crystals melt and re-crystallize, then melt again at 175 °C [33]. During the cooling cycle, the  $T_c$  remained constant at  $\sim 100$  °C for PLA as well as master batches G5 and P5, but the  $T_c$  of A5, B5, and Y5 was higher, with B5 showing the highest  $T_c$  of  $\sim 140$  °C. These data indicate that these colorants have a nucleating effect on PLA and thus promote crystallization. Similar nucleating effects have been observed in the past for compounds containing small amounts of pigment in a PP matrix and by talc and bis(hydroxyethyl)terephthalate in the case of PLA [34,35].

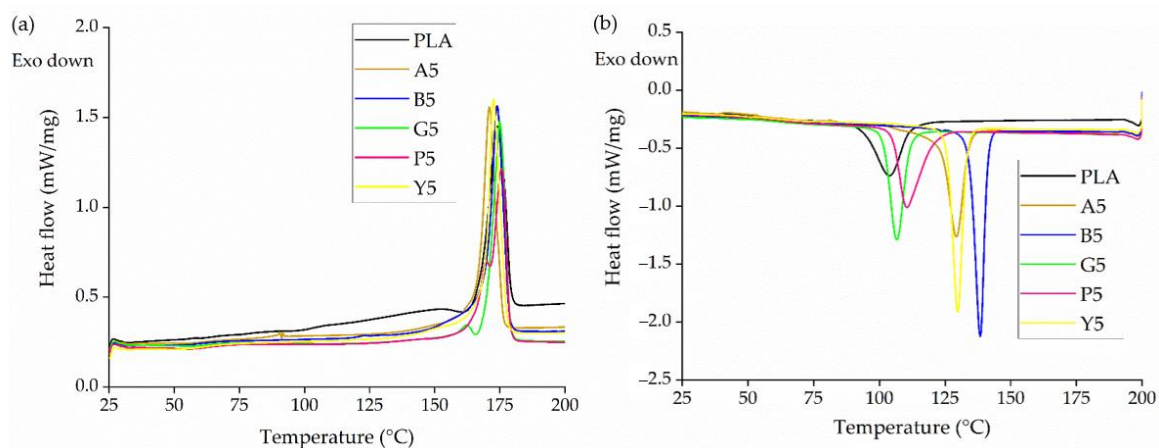


**Figure 4.** DSC thermograms of PLA and its master batches containing 5% (*w/w*) of each colorant during (a) the heating cycle and (b) the cooling cycle.

#### 3.2.2. Rheological Characteristics

The rheograms of PLA and its master batches containing 5% (*w/w*) of each colorant are presented in Figure 5. All six materials showed non-Newtonian shear thinning behavior, in

which the viscosity declines with increasing shear rate. This behavior is typical of polymers at high temperatures [36–38]. To facilitate a visual comparison, the complex viscosity of PLA and its master batches are shown at an angular frequency of 10/s in Figure 5b.

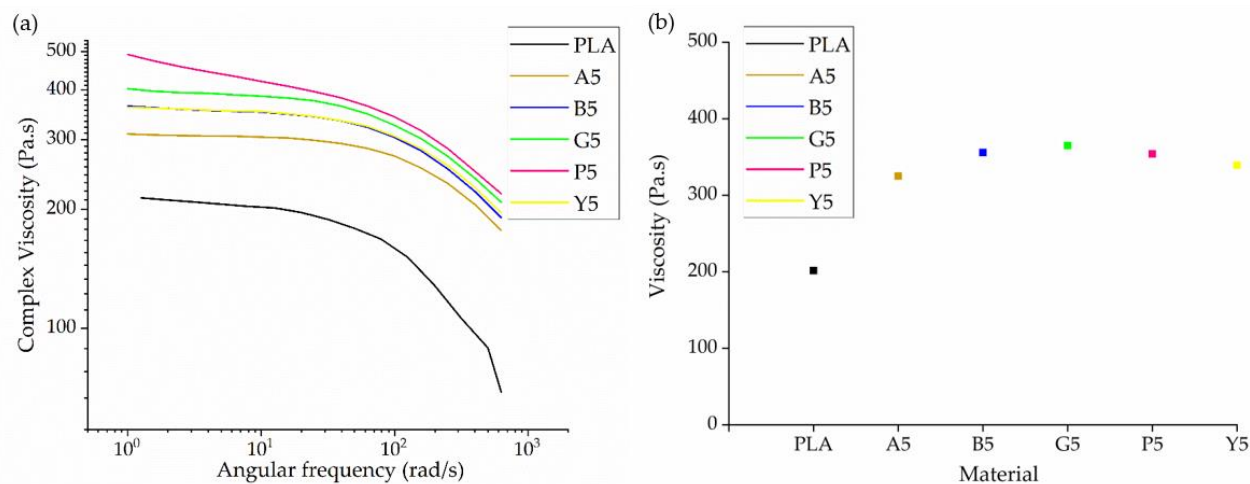


**Figure 5.** Rheological analysis of PLA and its master batches containing 5% (*w/w*) of each colorant. (a) Rheogram of PLA and the five master batches. (b) Complex viscosity of PLA and the five master batches at an angular frequency of 10/s.

The complex viscosity of PLA at an angular frequency of 10 rad/s was 201 Pa.s, but the value increased in the presence of each colorant. The highest increase of 47% was observed for master batch G5. Given that the colorants do not melt below 200 °C, they must act as anchors for the PLA chains, leading to an increase in melt viscosity. Furthermore, the polar groups in the colorants can interact with the polar groups in the PLA chain, hindering chain slippage and increasing the viscosity even further, as previously reported [22]. A similar increase in viscosity was reported when PLA was grafted with carbon black [39]. However, given the much lower weight percentage of colorants used for melt spinning (0.1–0.3%), we did not expect a substantial increase in viscosity or any effect on the behavior of the polymer.

### 3.2.3. Molecular Interactions between the Colorants and PLA

The FTIR spectra of PLA and its master batches were very similar (Figure 6). They all featured the characteristic C-H stretching peaks at 2993/cm and 2939/cm and C-O bending at 1184/cm. However, the peak at 1747/cm, representing the C=O stretching of PLA, shifted to 1750/cm in all of the master batches. This may signify an interaction between the hydroxyl groups of PLA and the functional groups of colorants, which could promote the distribution of colorant molecules in the PLA matrix. A similar shift in the C=O stretching peak of PLA was also observed when PLA was mixed with Kenaf fibers, indicating the possibility of hydrogen bonding between the components [40]. The hydrogen bonding observed in our FTIR spectra may explain the increase in the viscosity of the PLA master batches. In the case of the P5 master batch, we observe additional peaks between wavenumbers of 1650/cm and 1580/cm. This can be attributed to the bending vibration of the amine (N-H) group present in the pigment [41,42].

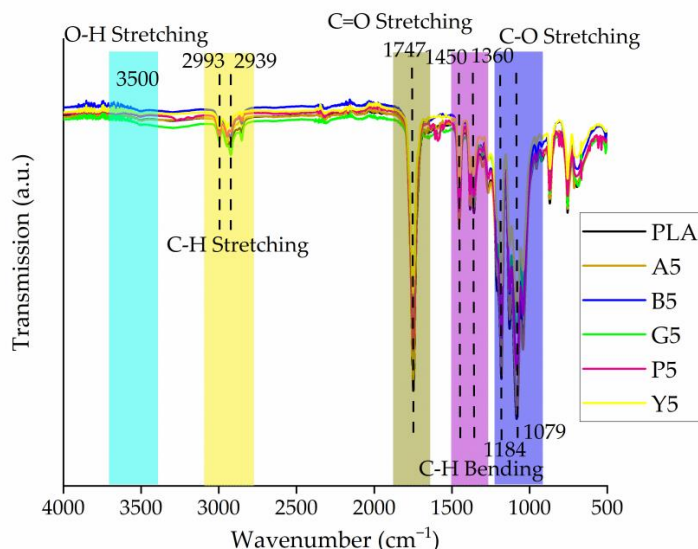


**Figure 6.** FTIR spectra of PLA and its master batches containing 5% (*w/w*) of each colorant.

### 3.2.4. Morphological Analysis

The dispersion of colorants in the PLA matrix was investigated by SEM. Cross-section images of PLA (after the compounding simulation step) and the master batches revealed that three colorants (alizarin, pigment blue 15:1, and pink PR122) were well dispersed (Figure 7). We only observed a few small aggregates ( $\sim 2 \mu\text{m}$ ) in these samples, including the pure PLA, suggesting that they represented additives introduced by the manufacturer. However, we find more agglomerates in case of the master batches made with green 7 and yellow 155. In Section 3.1.2, we observed that these two pigments have plate-like structure, and this leads to the hypothesis that these structures are harder to disperse in PLA. Still, this contrasts with our previous study, in which we observed more abundant aggregates for almost all colorants [22]. However, in the previous study, a glass syringe with a plunger was used for spinning. The compounds were filled and melted inside the syringe barrel, and no shear was applied to break down the aggregates. In contrast, we applied shear during the preparation of our master batches and melt spinning to improve the mixing of the colorants. Furthermore, the colorants used here (and PLA) dissolve in solvents such as chloroform and dimethyl formamide, suggesting the Hansen solubility parameter of the colorants and PLA matrix are similar. FTIR spectroscopy provided evidence for the formation of hydrogen bonds, which also supports the compatibility of the colorants with PLA [43].

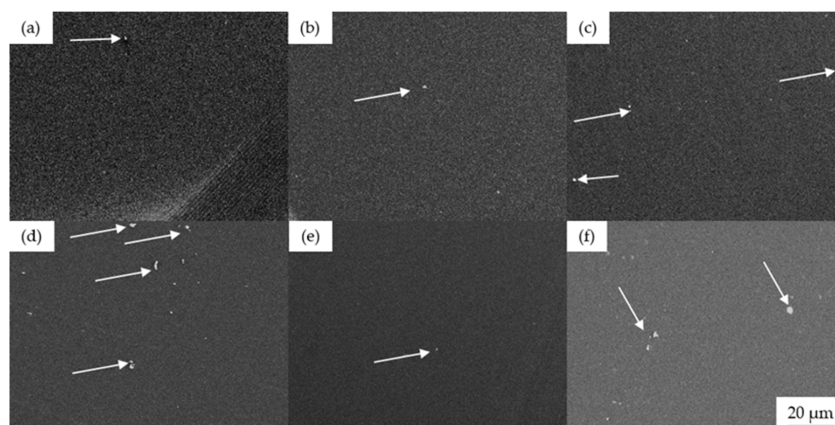


**Figure 7.** SEM images of cross-sectioned PLA and master batch granules: (a) pure PLA, (b) A5, (c) B5, (d) G5, (e) P5, and (f) Y5. Arrows indicate the position of aggregates.

### 3.2.5. GPC Analysis

GPC analysis revealed no significant difference in the molecular weight or PDI of PLA and its master batches (Figure 8). The relative  $M_w$  of PLA was 145,690 Da; the  $M_n$  was 83,016 Da; and the PDI was 1.76. A5 had the lowest  $M_w$  (131,950 Da) and  $M_n$  (78,316 Da), whereas P5 had the highest  $M_w$  (147,060 Da) and  $M_n$  (83,355 Da). The PDI of all samples was  $\sim 1.70$ . These data confirmed that the addition of colorants did not lead to the degradation of PLA and that dope dyeing therefore avoids the polymer chain degradation that is typically observed during conventional exhaust dyeing.

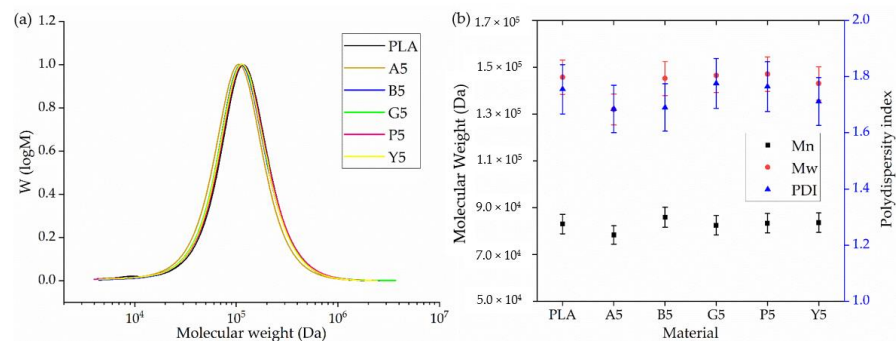


**Figure 8.** GPC analysis of PLA and its master batches containing 5% (*w/w*) of each colorant. (a) GPC elugram with normalized intensity on the y-axis. (b) Mean  $M_w$ ,  $M_n$ , and PDI values  $\pm$  SE ( $n = 3$ ).

### 3.3. Characterization of Yarns

#### 3.3.1. Mechanical Properties

The linear density of all yarns was measured to be  $300 \pm 5$  dtex and was therefore considered 300 dtex for the tests. The tensile force vs. elongation graphs of PLA were compared at different SSD ratios (Figure 9a). We also compared PLA and dyed yarns containing 0.3% (*w/w*) of each colorant at SSD ratios of 1, 2, and 3 (Figure 9b–d).

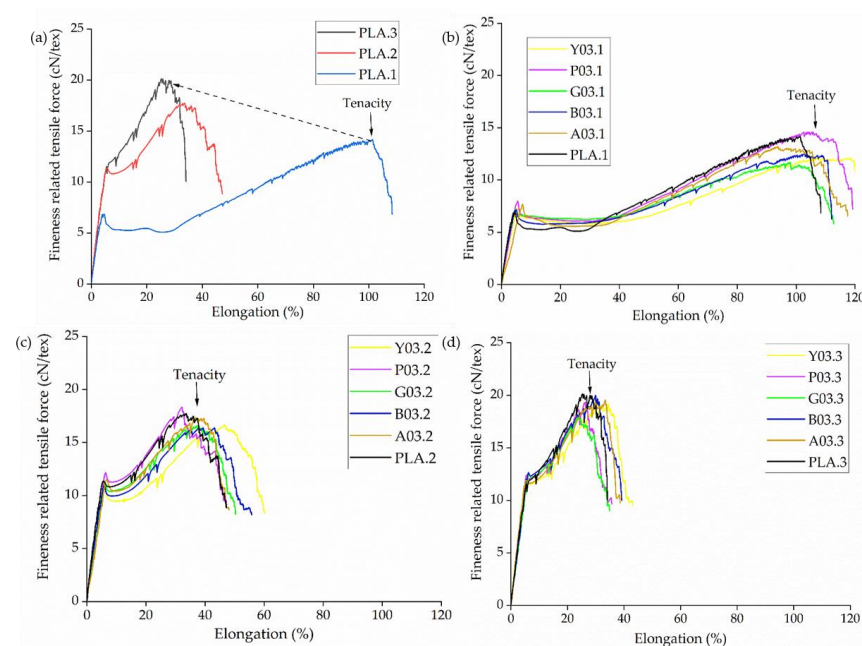


**Figure 9.** Tensilegrams of PLA and dyed yarns containing 0.3% (*w/w*) of each colorant at different SSD ratios. (a) Mean values of PLA yarns drawn at different SSD ratios. (b–d) Mean values of PLA and dyed yarns containing 0.3% (*w/w*) of each colorant drawn at SSD ratios of (b) 1, (c) 2, and (d) 3. Data are means of  $n = 5$  samples.

The tenacity (tensile strength) of PLA yarns increased at higher SSD ratios (Figure 9a). The tenacity increased by almost 50% (from 14 to 20 cN/tex) when the SSD ratio increased from 1 to 3. At the same time, the elongation declined by 72% (from 94% to 26%). Increasing the SSD ratio was previously shown to increase tenacity and reduce elongation by stretching and orienting the polymer chains, leading to strain-induced crystallization [44,45]. The mechanical properties obtained from melt spun PLA yarn are similar to the values obtained by researchers in the past, when a maximum tenacity of about 30 cN/tex was reported [46,47]. There was no significant change in the mechanical properties of the yarn in the presence of colorants (Table 3). For example, at an SSD ratio of 3, pure PLA yarns showed the highest tenacity (20.03 cN/tex) and Y03.3 yarns the lowest (18.30 cN/tex), whereas A03.3 yarns showed the greatest elongation (31%) and Y03.3 yarns the lowest (25%). The properties of all of the other yarns produced also fall in the same range. This is a significant advantage compared to conventional exhaust dyeing, in which the higher temperature and prolonged dyeing time reduce the mechanical integrity of PLA fabrics [6,48].

**Table 3.** Tenacity and elongation of PLA and dyed yarns containing 0.3% (*w/w*) of each colorant with standard deviations (SD).

Material	Tenacity (cN/tex)	Elongation at Maximum Force (%)
PLA.1	13.90 ± 0.57	94.33 ± 5.08
PLA.2	17.53 ± 0.32	36.33 ± 1.75
PLA.3	20.03 ± 0.17	26.33 ± 1.22
A03.1	13.20 ± 0.08	95.67 ± 2.50
A03.2	17.60 ± 0.20	39.33 ± 1.74
A03.3	19.97 ± 0.41	31.00 ± 1.63
B03.1	11.97 ± 0.37	97.33 ± 1.14
B03.2	17.03 ± 0.17	40.33 ± 1.12
B03.3	19.60 ± 0.51	27.33 ± 1.72
G01.1	13.07 ± 0.18	100.00 ± 4.23
G02.2	16.17 ± 0.40	39.67 ± 2.34
G03.3	19.33 ± 0.24	29.33 ± 0.98
P03.1	14.10 ± 0.37	100.00 ± 1.09
P03.2	16.63 ± 0.72	32.33 ± 0.42
P03.3	19.67 ± 1.18	25.00 ± 2.13
Y03.1	11.77 ± 0.16	95.00 ± 0.94
Y03.2	16.27 ± 0.34	34.00 ± 3.11
Y03.3	18.30 ± 0.38	25.33 ± 2.25

### 3.3.2. Physical Properties

Increasing the SSD ratio did not change the  $T_m$  of the yarns (Figure 10). However, although the  $T_g$  remained constant at SSD ratios of 1 and 2, no  $T_g$  peak was observed at an SSD ratio of 3 (Figure 10). The tenacity of the yarns increased by 20% when the SSD ratio increased from 1 to 2, but the increase in crystallinity was negligible (Table 3). This suggests that drawing during spinning was sufficient to orient the polymer chains but insufficient to induce crystallization. However, at an SSD ratio of 3, the increase in tenacity was accompanied by a >1.5-fold increase in the degree of crystallinity, reaching 51.7% for the pure PLA fibers. Such an increase in drawing leading to increased crystallinity, to a maximum of 67%, was also reported by Mai et al. [44,49] and was also anticipated because higher SSD ratios orient the polymer chains, creating a more ordered structure that induces crystallization during processing. We also observed a shoulder in the melting peak for PLA fibers at an SSD ratio of 3, probably reflecting the formation of imperfect  $\alpha'$  crystals during drawing, which melt at a temperature lower than  $\alpha$  crystals. Similar melting behavior has previously been observed for drawn PLA chains [44,49].

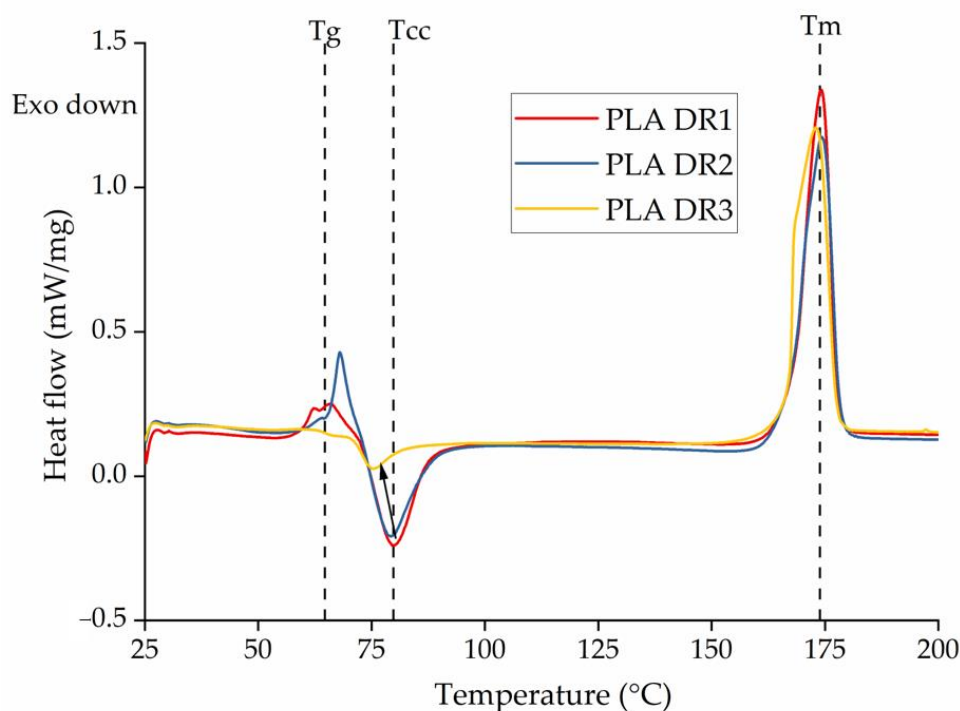


**Figure 10.** DSC thermogram of PLA yarns drawn at different ratios.

The higher crystallinity at an SSD ratio of 3 was also accompanied by a lower  $T_{cc}$ . Cold crystallization occurs due to rapid quenching, when amorphous polymer chains that cannot crystallize during spinning relax and crystallize to form a more ordered structure. Two hypotheses could explain the lower  $T_{cc}$ . First, the crystallinity of the yarns may be higher in PLA.3, limiting cold crystallization and therefore reducing the peak crystallization temperature. Second, the polymer chains are already oriented in yarns drawn with higher SSD ratios, so less energy is needed for crystallization, and cold crystallization is therefore accelerated. If the first hypothesis were correct, the onset of cold crystallization would remain constant regardless of the SSD ratio. We therefore tested for the onset of crystallization and found that the temperature declined from 75.7 °C (PLA.1) to 72.1 °C (PLA.2) and 70.8 °C (PLA.3) as the SSD ratio increased. Because the onset of crystallization also changes, the first hypothesis is rejected and the second hypothesis becomes more plausible. This leads to the conclusion that, among the parameters considered, the orientation resulting from SSD is higher than that resulting from melt drawing.

The DSC thermograms of pure PLA yarns and dyed yarns containing 0.3% ( $w/w$ ) of each colorant produced at different SSD ratios are presented in Figure 11, and the corresponding  $T_g$ ,  $T_m$ ,  $T_{cc}$ ,  $T_c$  and  $X_c$  values are summarized in Table 4. The DSC curves for dyed yarn containing 0.1% and 0.2% ( $w/w$ ) of each colorant were very similar and are provided in the appendix (Figures A1 and A2). As described above for the master batches (Section 3.2.1), the  $T_c$  increased in the presence of 0.3% ( $w/w$ ) of the blue 15:1 pigment and yellow 155 pigments because they act as strong nucleating agents. The  $T_c$  remained constant at 133 °C for the blue 15:1 pigment and 127 °C for the yellow 155 pigment, regardless of the weight percentage. Interestingly, although alizarin acted as a nucleating agent in master batch A5, the effect was not observed in the yarns, indicating that the nucleation effect only occurs at >0.3% ( $w/w$ ) alizarin.

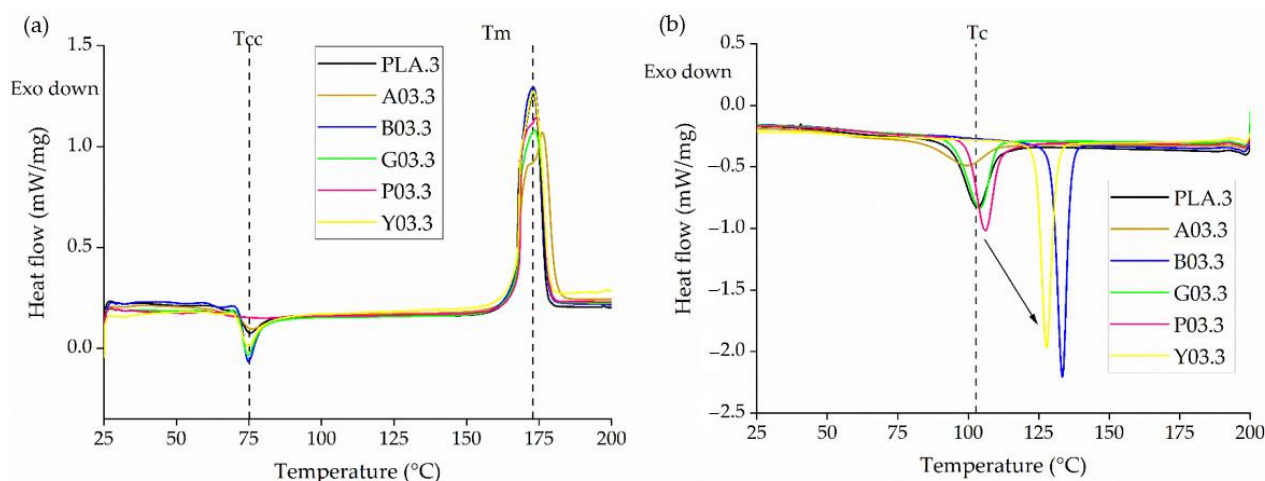


**Figure 11.** DSC thermogram of PLA and dyed yarns containing 0.3% (*w/w*) of each colorant at an SSD ratio of 3 during (a) the heating cycle and (b) the cooling cycle.

**Table 4.** The thermal transition values of PLA and dyed yarns drawn at different SSD ratios with SD ( $n = 3$ ).

Sample	$T_g$ (°C)	$T_{cc}$ (°C)	$T_m$ (°C)	$X_c$ (%)	$T_c$ (°C)
PLA.1	$60.8 \pm 0.2$	$79.5 \pm 0.5$	$174.2 \pm 0.9$	$29.8 \pm 2.1$	$100.2 \pm 0.5$
PLA.2	$60.5 \pm 0.5$	$79.3 \pm 0.6$	$174.3 \pm 0.6$	$29.9 \pm 1.3$	$100.2 \pm 1.3$
PLA.3	-	$75.0 \pm 0.1$	$173.0 \pm 1.0$	$51.7 \pm 3.1$	$100.2 \pm 0.9$
A03.1	$60.1 \pm 0.3$	$82.7 \pm 1.2$	$175.2 \pm 0.6$	$27.6 \pm 3.0$	$101.0 \pm 0.7$
A03.2	$60.5 \pm 0.1$	$81.3 \pm 1.7$	$174.9 \pm 1.0$	$29.7 \pm 1.7$	$97.7 \pm 1.5$
A03.3	-	$75.8 \pm 0.4$	$176.0 \pm 1.5$	$51.5 \pm 5.3$	$99.1 \pm 1.0$
B03.1	$60.2 \pm 1.5$	$84.3 \pm 0.8$	$174.4 \pm 0.3$	$30.7 \pm 0.8$	$133.1 \pm 0.4$
B03.2	$61.2 \pm 0.7$	$80.6 \pm 2.0$	$173.9 \pm 0.7$	$27.1 \pm 1.5$	$133.8 \pm 0.6$
B03.3	-	$74.8 \pm 0.3$	$172.8 \pm 0.4$	$48.5 \pm 3.1$	$133.4 \pm 0.8$
G03.1	$59.8 \pm 1.8$	$82.5 \pm 0.2$	$173.8 \pm 0.4$	$29.3 \pm 0.9$	$104.7 \pm 0.2$
G03.2	$60.2 \pm 1.9$	$79.8 \pm 1.3$	$174.6 \pm 0.6$	$30.4 \pm 0.9$	$105.2 \pm 0.2$
G03.3	-	$74.7 \pm 0.3$	$173.3 \pm 0.7$	$44.9 \pm 1.2$	$104.0 \pm 0.2$
P03.1	$60.0 \pm 0.5$	$79.9 \pm 0.7$	$174.6 \pm 0.1$	$29.9 \pm 1.9$	$108.7 \pm 1.4$
P03.2	$61.1 \pm 0.2$	$78.4 \pm 1.1$	$176.0 \pm 0.8$	$29.1 \pm 0.9$	$108.0 \pm 0.9$
P03.3	-	-	$173.7 \pm 0.2$	$52.1 \pm 0.1$	$106.2 \pm 0.6$
Y03.1	$60.2 \pm 3.2$	$82.8 \pm 0.5$	$174.6 \pm 0.1$	$29.7 \pm 0.3$	$127.2 \pm 1.0$
Y03.2	$61.8 \pm 0.3$	$79.9 \pm 1.5$	$174.3 \pm 0.8$	$30.0 \pm 1.3$	$127.5 \pm 0.9$
Y03.3	-	$74.8 \pm 0.5$	$173.1 \pm 0.2$	$48.47 \pm 2.1$	$127.7 \pm 1.0$

Table 3 also shows that the  $T_g$ ,  $T_m$ ,  $T_{cc}$ , and  $X_c$  values were unaffected by the presence of most colorants, but green 7 was an exception, with slightly lower values at an SSD of 3. However, the mechanical properties of the yarn were unchanged. This is probably because the colorant affects the crystallization process but does not interfere with polymer chain orientation. The degree of crystallinity of the yarns dyed with all other colorants drawn at an SSD ratio of 3 was 48–50%. This seems to be the case even for the blue 15:1 pigment and yellow 155 pigment showing nucleating effects. This is perhaps because DSC was carried out at lower cooling speeds of 10 °C/min, whereas higher cooling rates of >200 °C/s were applied during melt spinning. This suggests that, although some colorants act as strong nucleating agents at lower cooling rates, they do not have sufficient time to influence the crystallinity of the yarn during spinning. This differs from conventional dyeing, wherein changes in crystallinity are observed depending on the dyeing protocol. Only the green 7 colorant affected yarn crystallinity, but the effect was marginal and not enough to reduce mechanical strength. Dope dyeing is therefore advantageous because it offers better control over the crystallinity of the yarn.

### 3.3.3. Color and UV Stability

The CIE L\*a\*b color values and BWS of the PLA and dyed yarns revealed that increasing the weight percentage of colorant resulted in a darker shade of yarn (Table 5). This was indicated either by the L value (whiteness index), for example, in yarns containing alizarin, or by both the L and a values in the case of the green 7 colorant, because lower L values indicate darker colors and negative a values represent greener hues. All five colorants were stable on exposure to UV light, scoring  $\geq 7$  in the BWS test. Although the color obtained by the exhaust dyeing of PLA with natural colorants like alizarin and indigo was good, the light fastness of PLA exhaust dyed with alizarin was reported to be low in the past even when PLA was modified with nanoparticles, whereas the dope dyeing approach used herein led to improved light fastness [13,50,51].

**Table 5.** CIE L\*a\*b color values and blue wool scale (BWS) of PLA and dyed yarns.

Material	L	a	b	BWS
PLA-3	84.25	−0.42	2.23	$\geq 7$
A01-3	84.46	−2.8	22.19	-
A02-3	83.71	−4.12	41.78	-
A03-3	80.13	−2.67	53.66	$\geq 7$
B01-3	41.30	7.53	−31.81	-
B02-3	47.00	8.18	−32.21	-
B03-3	37.09	3.31	−25.22	$\geq 7$
G01-3	80.13	−25.83	1.66	-
G02-3	73.19	−43.85	3.44	-
G03-3	71.64	−51.32	3.62	$\geq 7$
P01-3	69.17	29.29	−14.61	-
P02-3	60.85	41.12	−19.52	-
P03-3	54.07	49.1	−22.34	$\geq 7$
Y01-3	85.06	−5.62	41.44	-
Y02-3	84.37	−4.94	30.93	-
Y03-3	85.77	−5.45	54.75	$\geq 7$

### 3.4. Characterization of Knitted Fabrics

#### 3.4.1. Water Vapor Permeability

Fabrics with greater water vapor permeability are considered to be more comfortable for daily use because they allow perspiration to evaporate [52]. The stitch density was kept constant in the knitting tests to avoid this parameter affecting the water vapor permeability [53]. We found that water vapor permeability was unaffected by the presence of colorants (Table 6). This agrees with previous studies of pigments added to silicone resin-based paints [54]. Water vapor permeability is affected by changes in the chemical structure, morphology, and surface characteristics of the fabric, which often occur during conventional dyeing because dye molecules needed to be fixed to the surface of fibers, thus ensuring color fastness. For example, a significant difference in water vapor permeability was reported, following the dyeing of cotton [55]. In contrast, dope dyeing involves the mixing of colorants with the polymer melt, causing the colorant to be distributed throughout the polymer matrix [18]. The absence of surface modification means that the water vapor permeability of knitted fabrics made from dyed PLA yarns is almost identical to that of pure PLA. It is also observed that the water vapor permeability of PLA fabric produced here is better than that of PET (reported to be 40%) and other PLA yarn (about 60%) reported in the past [56,57].

**Table 6.** Relative and absolute water vapor permeability of knitted fabrics made from PLA and dyed PLA yarns containing 0.3% (*w/w*) of colorants. Data are means  $\pm$  SD (*n* = 5).

Material	Relative Water Vapor Permeability (%)	Absolute Water Vapor Permeability (Pa/m <sup>2</sup> /W <sup>-1</sup> )
PLA	71.34 $\pm$ 3.04	2.60 $\pm$ 0.32
A03.1	70.30 $\pm$ 1.54	2.46 $\pm$ 0.19
B03.1	71.76 $\pm$ 3.16	2.72 $\pm$ 0.46
G03.1	73.56 $\pm$ 2.85	2.46 $\pm$ 0.35
P03.1	75.36 $\pm$ 2081	2.22 $\pm$ 0.32
Y03.1	74.60 $\pm$ 2.60	2.38 $\pm$ 0.31

### 3.4.2. Air Permeability

The flow of air through a knitted fabric is described as air permeability. Most colorants did not affect the air permeability of the knitted fabric, but the blue 15:1 colorant was an exception (Table 7). The blue 15:1 colorant reduced the air permeability slightly, although the change was not significant. The observed change could also reflect the use of laboratory-scale knitting equipment, which may introduce small irregularities. Our results differ from previous reports involving exhaust dyeing, wherein surface modifications that improve the incorporation of dyes in knitted fabrics can affect the air permeability of fabrics more significantly because the dyes form covalent bonds with the polymer chains [18,58]. Colorant molecules interact with the polymer via a different mechanism during dope dyeing, so we did not observe a similar effect. Dope dyeing therefore offers more scope to control the comfort properties of fabrics, including air permeability.

**Table 7.** Absolute air permeability of knitted fabrics made from PLA and dyed PLA yarns containing 0.3% (*w/w*) of each colorant. Data are means  $\pm$  SD (*n* = 5).

Material	Air Permeability (L/m <sup>2</sup> /s)
PLA	3848 $\pm$ 332
A03.1	3406 $\pm$ 65
B03.1	3026 $\pm$ 208
G03.1	3890 $\pm$ 116
P03.1	3506 $\pm$ 257
Y03.1	3906 $\pm$ 297

### 3.4.3. Martindale Abrasion Test

The first signs of abrasion were observed after 5000 cycles in the pure PLA fabrics, whereas more cycles (up to 10,000) were required to abrade the dyed fabrics (Figure 12 and Table 8). As stated above, these differences may reflect irregularities in the knitted surface introduced by the laboratory-scale knitting equipment. A value between 5000 and 10,000 cycles suggests that the fabrics produced here are more suited for decorative use (e.g., in cushions) than general use, which would require the fabrics to withstand >20,000 cycles [59]. Fabrics made from PLA blends have been reported to have low abrasion resistance, getting destroyed after 2250 cycles, but the yarn developed in this study was observed to have better abrasion resistance [60]. This can be the case because the yarn produced here had better mechanical properties compared to the PLA blend yarn used in the previous study. The processing conditions should therefore be optimized further to improve the abrasion resistance.

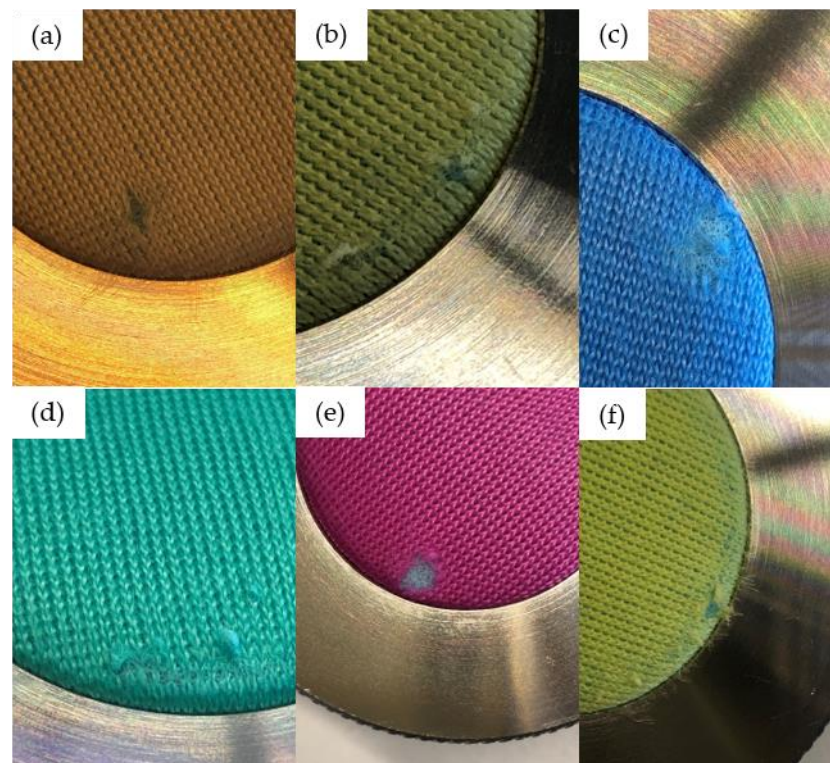


**Figure 12.** First signs of abrasion in knitted PLA fabrics: (a) PLA.1, (b) A03.1, (c) B03.1, (d) G03.1, (e) P03.1, and (f) Y03.1.

**Table 8.** Abrasion resistance and color fastness of PLA and dyed fabrics containing 0.3% (*w/w*) of each colorant, determined using the Martindale abrasion test.

Material	Abrasion Resistance (Number of Cycles)	Before Martindale			After Martindale		
		L	a	b	L	a	b
PLA	5000	78.50	−0.21	1.02	72.66	−1.47	3.67
A03.1	10,000	76.80	−2.15	45.20	63.36	−1.00	25.51
B03.1	7500	31.09	3.22	26.22	30.22	5.13	28.66
G03.1	10,000	65.22	−38.22	2.12	63.11	−35.56	2.25
P03.1	7500	44.94	50.05	−13.27	42.91	38.06	−13.23
Y03.1	7500	73.97	−11.13	40.77	70.23	−9.48	33.64

It is observed from Table 8 that the color fastness of PLA and the fabrics containing blue, green, pink, and yellow pigment is good. There was minimal color change after the Martindale abrasion test. However, in the case of fabric containing alizarin, a significant color change was observed and the fabric change from yellow to a light yellow color. The overall L,a,b values obtained herein are a little different from the values obtained from the yarn values. This could be the case because of the difference in the measurement method. In the case of yarn, the yarn was bundled into a ball, and the color was measured, and in the case of fabric, the color was measured directly from the reflection of light. This is hypothesized to lead to the small difference in color observed.

#### 4. Conclusions

We investigated the effect of colorants on the structure and properties of dope-dyed PLA yarn and fabric. We produced master batches of PLA containing 5% (*w/w*) of each colorant using a twin-screw compounder and generated PLA yarns containing up to 0.3% (*w/w*) of the colorants using a pilot-scale melt spinning machine. This is a more efficient and less environmentally harmful approach to dye thermolabile biopolymers such as PLA.

During spinning, we kept the winding speed constant but varied the melt composition and SSD ratio to investigate the effect of these parameters on the properties of PLA yarns. First, we analyzed the thermal properties and morphology of the colorants and found that no thermal transition occurred below the spinning temperature of 200 °C. We then analyzed the master batches to investigate the effect of colorants on the rheological and thermal properties of PLA, including its degradation. We observed that the presence of 5% (*w/w*) of the colorants led to an increase in viscosity. Furthermore, alizarin and the blue 15:1 and yellow 155 pigments showed nucleating activity. No change in molecular weight was observed in the master batches, suggesting the absence of PLA degradation. FTIR spectra revealed the possibility of hydrogen bonding between PLA and the colorants, which facilitated their distribution in the PLA matrix, as confirmed by SEM.

The mechanical testing of pure PLA yarns and yarns containing up to 0.3% (*w/w*) of the colorants spun at different drawing speeds revealed that the mechanical properties were affected most by the drawing speed, while the colorant had a negligible effect. Increasing the SSD ratio from 1 to 3 at a constant winding speed caused the tenacity of the yarn to increase by ~50%. DSC also revealed that drawing had a stronger influence on the degree of crystallinity of the yarns, but the colorant had no effect even if it acted as a nucleating agent. This may reflect the slow cooling rate during DSC (10 °C/min) compared to >200 °C/s during melt spinning, which is too rapid for nucleation to affect crystallization. Interestingly, the  $T_{cc}$  declined with increasing SSD ratio, suggesting that crystallization accelerates when there is already inherent orientation present in the processed yarn.

The BWS test revealed that all five colorants are UV-resistant. Furthermore, the incorporation of colorants had no effect on air permeability or water vapor permeability. The Martindale abrasion test revealed that the fabrics were suitable for decorative use. In conventional exhaust dyeing, the dyeing temperature and duration influence the mechanical properties, crystallinity, and the other physical aspects of knitted fabrics. In contrast, dope dyeing had little impact, allowing a greater degree of control over the yarn and fabric properties by modifying the process parameters. We also found that the potentially biobased colorant alizarin and the biobased pink PR122 pigment perform as well as the commercial colorants. We conclude that dope dyeing with colorants can be a sustainable alternative to conventional exhaust dyeing and offers better control of yarn properties.

**Author Contributions:** Conceptualization, N.K.B. and S.S.; methodology, N.K.B. and S.S.; software, N.K.B.; validation, N.K.B. and S.S.; formal analysis, N.K.B., S.S. and C.R.; investigation, N.K.B., S.S. and C.R.; resources, G.S. and R.G.; data curation, N.K.B., S.S. and C.R.; writing—original draft preparation, N.K.B.; writing—review and editing, N.K.B., S.S., C.R., R.G. and G.S.; visualization, N.K.B.; supervision, R.G. and G.S.; project administration, N.K.B.; funding acquisition, G.S. All authors have read and agreed to the published version of the manuscript.

**Funding:** This research was funded by the NWO under project number RAAK.PRO02.107.

**Institutional Review Board Statement:** Not applicable.

**Informed Consent Statement:** Not applicable.

**Data Availability Statement:** The datasets used and/or analyzed during this study are available from the corresponding author on reasonable request.

**Acknowledgments:** We would like to thank our laboratory technician Henri Becker for the maintenance and modification of our equipment and our student Konrad Beukenberg for supporting the experimental trial preparations. We would like to extend our gratitude to Richard M Twyman for his extensive support with language corrections. We would also like to thank Dorien Derksen and Eric Mattheussens for offering assistance with color measurements.

**Conflicts of Interest:** The authors declare no conflict of interest.

## Appendix A

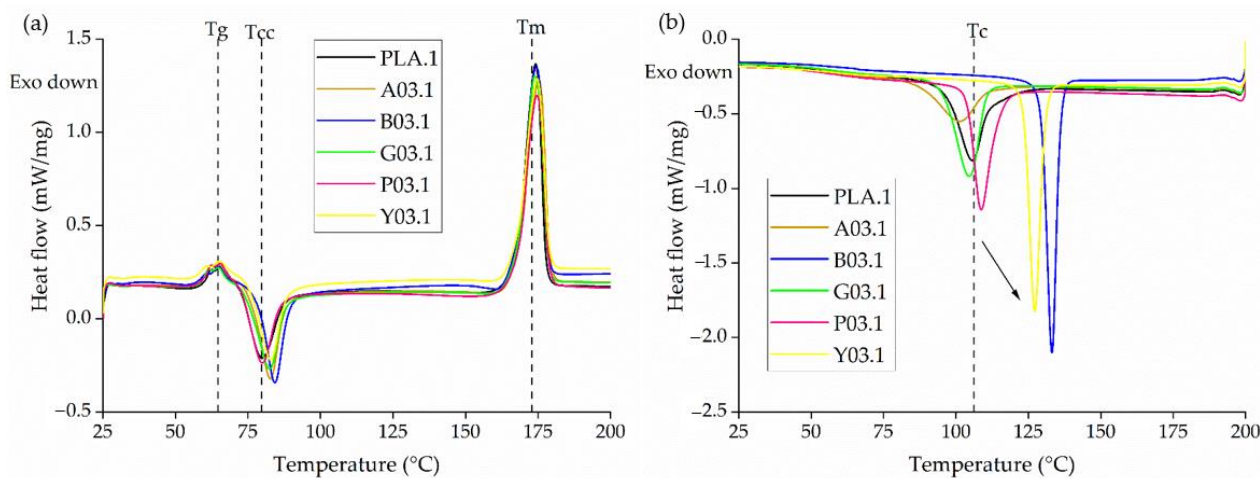


**Figure A1.** DSC thermograms of PLA and dyed yarns containing 0.3% (*w/w*) of each colorant at an SSD ratio of 1 during (a) the heating cycle and (b) the cooling cycle.

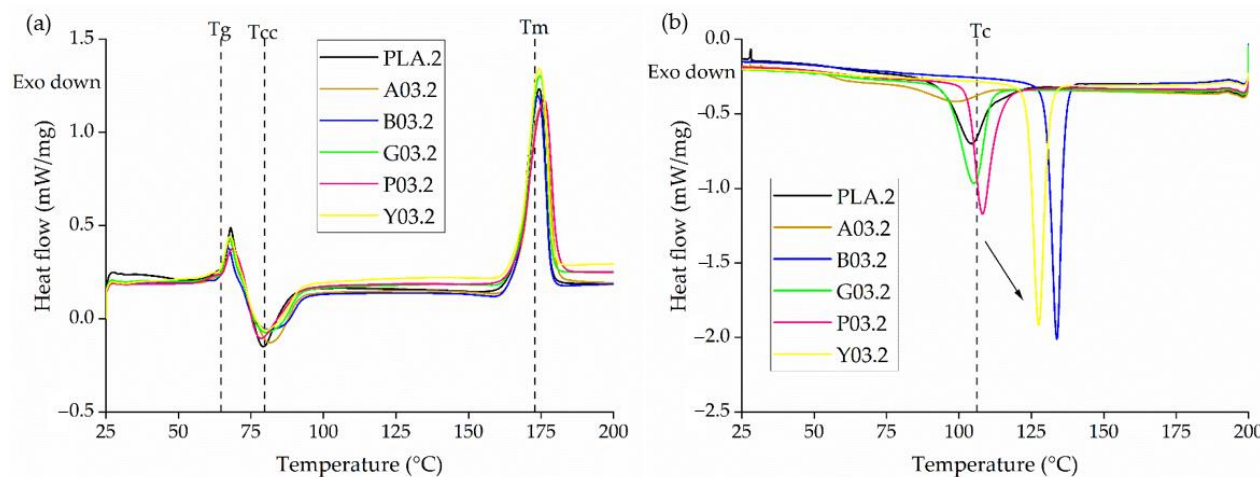


**Figure A2.** DSC thermograms of PLA and dyed yarns containing 0.3% (*w/w*) of each colorant at an SSD ratio of 2 during (a) the heating cycle and (b) the cooling cycle.

## References

1. Pulidini, K.B.S. Polyester Fiber Market Size. Available online: <https://www.gminsights.com/industry-analysis/polyester-fiber-market> (accessed on 2 May 2022).
2. Carus, M. Nova-Institute Announces New Market Study on Bioplastics with Latest Data for 2018. Available online: <https://renewable-carbon.eu/news/nova-institute-announces-new-market-study-on-bioplastics-with-latest-data-for-2018/> (accessed on 18 November 2022).
3. Hussain, T.; Tausif, M.; Ashraf, M. A review of progress in the dyeing of eco-friendly aliphatic polyester-based polylactic acid fabrics. *J. Clean. Prod.* **2015**, *108*, 476–483. [[CrossRef](#)]
4. Chen, G.Q.; Patel, M.K. Plastics derived from biological sources: Present and future: A technical and environmental review. *Chem. Rev.* **2012**, *112*, 2082–2099. [[CrossRef](#)] [[PubMed](#)]
5. Abdrabbo, A.; El-Dessouky, H.M.; Fotheringham, A.F. Treatment of polylactic acid fibre using low temperature plasma and its effects on vertical wicking and surface characteristics. *J. Text. Inst.* **2013**, *104*, 28–34. [[CrossRef](#)]
6. Xu, S.; Chen, J.; Wang, B.; Yang, Y. Sustainable and Hydrolysis-Free Dyeing Process for Polylactic Acid Using Nonaqueous Medium. *ACS Sustain. Chem. Eng.* **2015**, *3*, 1039–1046. [[CrossRef](#)]
7. Ma, P.; Xu, Y.; Wang, D.; Dong, W.; Chen, M. Rapid crystallization of poly(lactic acid) by using tailor-made oxalamide derivatives as novel soluble-type nucleating agents. *Ind. Eng. Chem. Res.* **2014**, *53*, 12888–12892. [[CrossRef](#)]
8. Wang, L.; Wang, Y.-n.; Huang, Z.-g.; Weng, Y.-x. Heat resistance, crystallization behavior, and mechanical properties of polylactide/nucleating agent composites. *Mater. Des. (1980–2015)* **2015**, *66*, 7–15. [[CrossRef](#)]

9. Baig, G.A. Hydrolytic stability of PLA yarns during textile wet processing. *Fibers Polym.* **2013**, *14*, 1912–1918. [CrossRef]
10. Bayati, S.; Tavanaie, M.A. Dyeing of recycled Poly(lactic acid) fibers from disposable packages flake with low energy consumption and effluent. *J. Clean. Prod.* **2018**, *176*, 382–390. [CrossRef]
11. Fattahi, F.; Izadan, H.; Khodammi, A. Investigation into the Effect of UV/Ozone Irradiation on Dyeing Behaviour of Poly(Lactic Acid) and Poly(Ethylene Terephthalate) Substrates. *Prog. Color Color. Coat.* **2012**, *5*, 7.
12. Sidarkote, R.; Suwanruji, P.; Suesat, J. Exhaust Dyeing Poly(Lactic Acid) Fabrics with Indigo Dye Obtained from *Indigofera Tinctoria*. *Adv. Mater. Res.* **2014**, *1025–1026*, 531–534. [CrossRef]
13. Baykuş, O.; Tugce Celik, I.; Dogan, S.D.; Davulcu, A.; Dogan, M. Enhancing the dyeability of poly(lactic acid) fiber with natural dyes of alizarin, lawsone, and indigo. *Fibers Polym.* **2017**, *18*, 1906–1914. [CrossRef]
14. Fajraoui, A.; Ben Nasr, J.; Lacoste, C.; Amar, M.B.; Dony, P.; Odof, S.; El Halouani, F. Coloration of the polylactic acid with the natural dye extracted from acacia cyanophylla flowers. *Polym. Test.* **2019**, *78*, 105988. [CrossRef]
15. Mogi, K.; Kubokawa, H.; Hatakeyama, T. Effect of dyeing on melting behavior of poly(lactic acid) fabric. *J. Therm. Anal. Calorim.* **2002**, *70*, 867–875. [CrossRef]
16. Carmen, Z.; Daniela, S. Textile Organic Dyes—Characteristics, polluting effects and separation/elimination procedures from industrial effluents—A critical overview. In *Organic Pollutants Ten Years After the Stockholm Convention*; Puzyn, T., Mostrag-Szlichtyng, A., Eds.; InTech: Rang-Du-Fliers, France, 2012; Volume 1, pp. 55–86.
17. Carmichael, A. Man-Made Fibers Continue To Grow. Available online: <https://www.textileworld.com/textile-world/fiber-world/2015/02/man-made-fibers-continue-to-grow/> (accessed on 2 May 2022).
18. Choudhury, A.K.R. *Handbook of Textile and Industrial Dyeing*; Woodhead Publishing: Cambridge, UK, 2011; Volume 2.
19. Zhang, L.; Dong, H.; Li, M.; Wang, D.; Liu, M.; Wang, C.; Fu, S. Synthesis and characterization of carbon black modified by polylactic acid (PLA-g-CB) as pigment for dope dyeing of black PLA fibers. *J. Appl. Polym. Sci.* **2019**, *137*, 48784. [CrossRef]
20. Reinhardt, D. *Vergleichende Sachbilanz im Textilbereich—Spinnfärbung versus Flottenfärbung*; Friedrich-Schiller-Universität: Jena, Germany, 2003; p. 5.
21. Tavanaie, H.; Morshed, M.; Zarebini, M.; Salehi, R.A. A Study of the Nucleation Effect of Pigment Dyes on the Microstructure of Mass Dyed Bulked Continuous Filament Polypropylene. *Iran. Polym. J.* **2005**, *14*, 267–276.
22. Balakrishnan, N.K.; Koenig, K.; Seide, G. The effect of dye and pigment concentrations on the diameter of melt-electrospun polylactic acid fibers. *Polymers* **2020**, *12*, 2321. [CrossRef] [PubMed]
23. Pigment Blue 15. Available online: <https://www.tcichemicals.com/NL/nl/p/P0655> (accessed on 12 November 2022).
24. Henan Tianfu Chemical Co., Ltd. Pigment Green 7. Available online: [https://www.chemicalbook.com/ProductChemicalPropertiesCB7399460\\_EN.htm#MSDSA](https://www.chemicalbook.com/ProductChemicalPropertiesCB7399460_EN.htm#MSDSA) (accessed on 12 November 2022).
25. Pigment Red 122. Available online: <https://www.additivesforpolymer.com/portfolio/pigment-red-122/> (accessed on 12 November 2022).
26. Pigment Yellow 155. Available online: <https://pubchem.ncbi.nlm.nih.gov/compound/Pigment-Yellow-155> (accessed on 12 November 2022).
27. Alizarin. Available online: <https://www.sigmaaldrich.com/catalog/product/sial/122777?lang=en&region=NL> (accessed on 12 November 2022).
28. Jia, S.; Yu, D.; Zhu, Y.; Wang, Z.; Chen, L.; Fu, L. Morphology, crystallization and thermal behaviors of PLA-based composites: Wonderful effects of hybrid GO/PEG via dynamic impregnating. *Polymers* **2017**, *9*, 528. [CrossRef]
29. Pyda, M.; Bopp, R.C.; Wunderlich, B. Heat capacity of poly(lactic acid). *J. Chem. Thermodyn.* **2004**, *36*, 731–742. [CrossRef]
30. Zhang, H.; Bai, H.; Liu, Z.; Zhang, Q.; Fu, Q. Toward high-performance poly(l-lactide) fibers via tailoring crystallization with the aid of fibrillar nucleating agent. *ACS Sustain. Chem. Eng.* **2016**, *4*, 3939–3947. [CrossRef]
31. Sohn, J.R.; Han, J.S. NiO-TiO<sub>2</sub> Catalyst Modified with WO<sub>3</sub> for Ethylene Dimerization. In *New Developments and Application in Chemical Reaction Engineering*; Rhee, H.K., Nam, I.S., Park, J.P., Eds.; Studies in Surface Science and Catalysis; Elsevier B.V.: Amsterdam, The Netherlands, 2006; Volume 159, pp. 269–272.
32. Marzec, A. The effect of dyes, pigments and ionic liquids on the properties of elastomer composites. Ph.D. Thesis, Technical university of Lodz, Łódź, Poland, University Claude Bernard-Lyon 1, Villeurbanne, France, 2014.
33. Gracia-Fernández, C.A.; Gómez-Barreiro, S.; López-Beceiro, J.; Naya, S.; Artiaga, R. New approach to the double melting peak of poly(l-lactic acid) observed by DSC. *J. Mater. Res.* **2012**, *27*, 1379–1382. [CrossRef]
34. Lee Wo, D.; Tanner, R.I. The impact of blue organic and inorganic pigments on the crystallization and rheological properties of isotactic polypropylene. *Rheol. Acta* **2009**, *49*, 75–88. [CrossRef]
35. Yu, F.; Liu, T.; Zhao, X.; Yu, X.; Lu, A.; Wang, J. Effects of talc on the mechanical and thermal properties of polylactide. *J. Appl. Polym. Sci.* **2012**, *125*, E99–E109. [CrossRef]
36. Dorgan, R.J. *Poly(lactic acid): Synthesis, Structures, Properties, Processing, Applications, and End of Life*, 2nd ed.; Grossman, F.R.N.D., Ed.; John Wiley & Sons, Inc.: Hoboken, NJ, USA, 2022.
37. Bourg, V.; Valette, R.; Le Moigne, N.; Ienny, P.; Guillard, V.; Bergeret, A. Shear and extensional rheology of linear and branched polybutylene succinate blends. *Polymers* **2021**, *13*, 652. [CrossRef] [PubMed]
38. Fang, Q.; Hanna, M.A. Rheological properties of amorphous and semicrystalline polylactic acid polymers. *Ind. Crops Prod.* **1999**, *10*, 47–53. [CrossRef]

39. Zhang, L.; Dong, H.; Li, M.; Wang, L.; Liu, Y.; Wang, L.; Fu, S. Fabrication of polylactic acid-modified carbon black composites into improvement of levelness and mechanical properties of spun-dyeing polylactic acid composites membrane. *ACS Sustain. Chem. Eng.* **2018**, *7*, 688–696. [CrossRef]
40. Kamarudin, S.H.; Chuah, A.L.; Aung, M.M.; Ratnam, C.T.; Jusoh, E.R. A study of mechanical and morphological properties of PLA based biocomposites prepared with EJO vegetable oil based plasticiser and kenaf fibres. *Mater. Res. Express* **2018**, *5*, 085314. [CrossRef]
41. Zhu, H.; Peng, S.; Jiang, W. Electrochemical properties of PANI as single electrode of electrochemical capacitors in acid electrolytes. *Sci. World J.* **2013**, *2013*, 940153. [CrossRef]
42. LibreTexts. Infrared Spectroscopy Absorption Table. Available online: [https://chem.libretexts.org/Ancillary\\_Materials/Reference/Reference\\_Tables/Spectroscopic\\_Reference\\_Tables/Infrared\\_Spectroscopy\\_Absorption\\_Table](https://chem.libretexts.org/Ancillary_Materials/Reference/Reference_Tables/Spectroscopic_Reference_Tables/Infrared_Spectroscopy_Absorption_Table) (accessed on 12 November 2022).
43. David, D.J.; Sincock, T.F. Estimation of miscibility based on solubility parameter concept. *Polymer* **1991**, *33*, 4506–4514.
44. Siebert, S.; Berghaus, J.; Seide, G. Nucleating agents to enhance poly(l-Lactide) fiber crystallization during industrial-scale melt spinning. *Polymers* **2022**, *14*, 1395. [CrossRef]
45. Baird, D.G.; Collias, D.I. *Polymer Processing: Principles and Design*, 2nd ed.; John Wiley & Sons, Inc.: Hoboken, NJ, USA, 2014.
46. Naeimirad, M.; Zadhoush, A.; Esmaeely Neisiany, R.; Salimian, S.; Kotek, R. Melt-spun PLA liquid-filled fibers: Physical, morphological, and thermal properties. *J. Text. Inst.* **2018**, *110*, 89–99. [CrossRef]
47. Olmen, R.V. Biobased PLA Yarns with High Mechanical Properties. Available online: <https://www.centexbel.be/en/news/biobased-pla-yarns-with-high-mechanical-properties> (accessed on 18 September 2022).
48. Phillips, D.; Suesat, J.; Wilding, M.; Farrington, D.; Sandukas, S.; Sawyer, D.; Bone, J.; Dervan, S. Influence of different preparation and dyeing processes on the physical strength of the Ingeo<sup>+</sup> fibre component in an Ingeo fibre/cotton blend. Part 1: Scouring followed by dyeing with disperse and reactive dyes. *Color. Technol.* **2004**, *120*, 35–40. [CrossRef]
49. Mai, F.; Tu, W.; Bilotti, E.; Peijs, T. The Influence of Solid-State Drawing on Mechanical Properties and Hydrolytic Degradation of Melt-Spun Poly(Lactic Acid) (PLA) Tapes. *Fibers* **2015**, *3*, 523–538. [CrossRef]
50. Ujjin, S.; Jantip, S. Study on the dyeing properties of poly(lactic acid) and silk yarns with natural dyes. *Adv. Mater. Res.* **2012**, *486*, 384–387. [CrossRef]
51. Drivas, I.; Blackburn, R.S.; Rayner, C.M. Natural anthraquinonoid colorants as platform chemicals in the synthesis of sustainable disperse dyes for polyesters. *Dye. Pigment.* **2011**, *88*, 7–17. [CrossRef]
52. Praharn, C.; Barker, R.L.; Gupta, B.S. Moisture vapor transport behavior of polyester knit fabrics. *Text. Res. J.* **2016**, *75*, 346–351. [CrossRef]
53. Gupta, D.; Kothar, V.K.; Jhanj, Y. Heat and moisture transport in single jersey plated fabrics. *Indian J. Fibre Text. Res.* **2013**, *39*, 7.
54. Lisowski, J.; Szadkowski, B.; Marzec, A. Effects of selected pigments on the properties of silicone resin-based paints. *Materials* **2022**, *15*, 4961. [CrossRef]
55. Shu, D.; Fang, K.; Liu, X.; Cai, Y.; An, F.; Qu, G.; Liang, Y. Cleaner pad-steam dyeing technology for cotton fabrics with excellent utilization of reactive dye. *J. Clean. Prod.* **2019**, *241*, 118370. [CrossRef]
56. Demiryürek, O.; Uysaltürk, D. Thermal comfort properties of Viloft/cotton and Viloft/polyester blended knitted fabrics. *Text. Res. J.* **2013**, *83*, 1740–1753. [CrossRef]
57. Maqsood, M.; Seide, G. Development of biobased socks from sustainable polymer and statistical modeling of their thermo-physiological properties. *J. Clean. Prod.* **2018**, *197*, 170–177. [CrossRef]
58. Ho-Jin, N.; Dong-Won, J.; Jong-Jun, K. Effect of Mordanting, Dyeing, Rinsing, and Fiber Characteristics on the Air-permeability and Color of Fabrics Dyed using Cochineal Dyestuff. *J. Fash. Bus.* **2005**, *9*, 114–124.
59. Alice. The Martindale Test: Fabric Rub Count. Available online: <https://www.justfabrics.co.uk/inspiration/the-martindale-test-fabric-rub-count/> (accessed on 18 November 2022).
60. Huang, X.X.; Tao, X.M.; Zhang, Z.H.; Chen, P. Properties and performances of fabrics made from bio-based and degradable polylactide acid/poly (hydroxybutyrate- co-hydroxyvalerate) (PLA/PHBV) filament yarns. *Text. Res. J.* **2016**, *87*, 2464–2474. [CrossRef]